energies

MDPI

Article

Development of a Biomass Component Prediction Model Based on Elemental and Proximate Analyses

Sun Yong Park [1,†], Kwang Cheol Oh [2,†], Seok Jun Kim [1], La Hoon Cho [1], Young Kwang Jeon [1] and DaeHyun Kim [1,3,*]

[1] Department of Interdisciplinary Program in Smart Agriculture, Kangwon National University, Hyoja 2 Dong 192-1, Chuncheon 24341, Republic of Korea; ksj91@kangwon.ac.kr (S.J.K.); jjola1991@kangwon.ac.kr (L.H.C.); glorysmith@daum.net (Y.K.J.)
[2] Agriculture and Life Science Research Institute, Kangwon National University, Hyoja 2 Dong 192-1, Chuncheon 24341, Republic of Korea
[3] Department of Biosystems Engineering, Kangwon National University, Hyoja 2 Dong 192-1, Chuncheon 24341, Republic of Korea
* Correspondence: daekim@kangwon.ac.kr; Tel.: +82-33-250-6496
† These authors contributed equally to this work.

Abstract: Emerging global environmental pollution issues have caused a reduction in coal utilization, leading to an increased research focus on biomass use as an alternative. However, due to the low heat values of biomass, studies in this field are still in progress. Biomass primarily comprises cellulose, hemicellulose, and lignin. To determine the composition of these three components, the measurement methods recommended by TAPPI (Technical Association of the Pulp and Paper Industry) and NREL (National Renewable Energy Laboratory) are typically employed involving equipment such as HPLC. However, these methods are time consuming. In this study, we proposed a model for predicting cellulose, hemicellulose, and lignin contents based on elemental and industrial analyses. A dataset comprising 174 samples was used to develop this model. This was validated using 25 additional samples. The R^2_P values for cellulose, hemicellulose, and lignin were 0.6104–0.6362, 0.4803–0.5112, and 0.7247–0.7914, respectively; however, the R^2_{CV} values obtained from the validation results were 0.7387–0.7837, 0.3280–0.4004, and 0.7427–0.7757, respectively. The optimal models selected for cellulose, lignin, and hemicellulose were C1, L2, and 100-(C1-L2) or H2, respectively. Our predictions for woody and herbaceous biomass, including torrefied samples, should be applied with caution to other biomass types due to the potential accuracy limitations. To enhance the prediction accuracy, future research should broaden the range of biomass types considered and gather more data specifically related to woody and herbaceous biomass.

Keywords: pollution; coal; energy; biomass

check for updates

Citation: Park, S.Y.; Oh, K.C.; Kim, S.J.; Cho, L.H.; Jeon, Y.K.; Kim, D. Development of a Biomass Component Prediction Model Based on Elemental and Proximate Analyses. *Energies* **2023**, *16*, 5341. https://doi.org/10.3390/en16145341

Academic Editors: Dimitrios Sidiras, Nepu Saha and Jordan Klinger

Received: 22 May 2023
Revised: 4 July 2023
Accepted: 10 July 2023
Published: 13 July 2023

Copyright: © 2023 by the authors. Licensee MDPI, Basel, Switzerland. This article is an open access article distributed under the terms and conditions of the Creative Commons Attribution (CC BY) license (https://creativecommons.org/licenses/by/4.0/).

1. Introduction

As interest in the environment is on the rise, much research is being conducted on alternative renewable energy sources to replace traditional fossil fuels. In particular, research has been conducted on alternative energy sources, such as hydrogen energy and batteries, which are currently prevalent. Globally, there is a strong reliance on thermal power generation to generate large amounts of electricity. This has caused increasing interest in biomass power plants that use biofuels as an alternative to coal. The use of agricultural and forest-based biomass is particularly advantageous because it is continuously produced by human activities and is relatively evenly distributed worldwide, unlike fossil fuels, which are concentrated in specific regions. However, biomass has been criticized for its high ash content and low calorific value compared with fossil fuels. To address these drawbacks, various thermochemical conversion processes have been conducted. In particular, processes such as torrefaction and carbonization have been developed to use

biomass as a solid fuel. During the thermochemical conversion of biomass, the contents of the three components of biomass—cellulose, hemicellulose, and lignin—are important. Cellulose (Figure 1) is a glucose polymer with the structure $[C_6H_{10}O_5]_n$ [1]. Hemicellulose (Figure 2) is a complex of 6-carbon and 5-carbon sugars, primarily composed of arabinose, xylose, mannose, galactose, and glucose [2]. In contrast, lignin comprises three phenylpropanoid units (p-coumaryl, coniferyl, and sinapyl alcohols) derived from cinnamyl alcohol (Figure 3) [3].

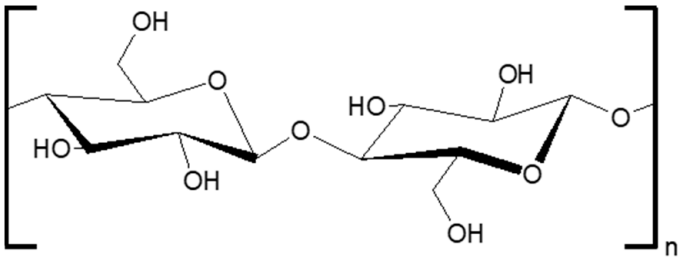


Figure 1. Structure of cellulose.

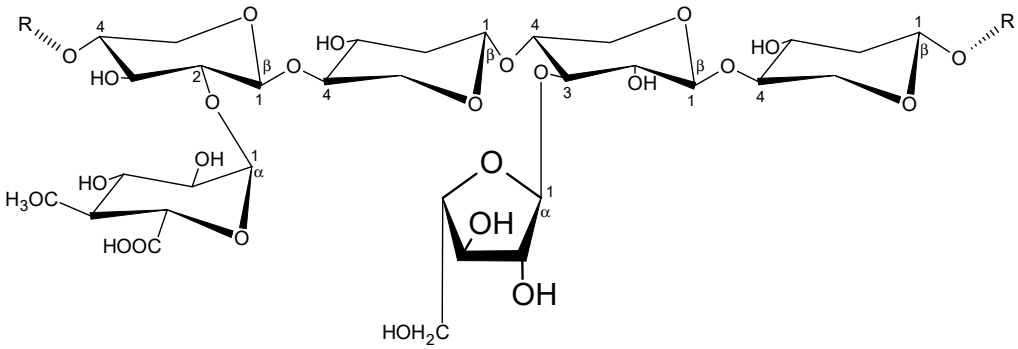


Figure 2. Structure of hemicellulose consisting of a xylopyranose backbone with glucuronic acid (1→2) and arabinofuranose (1→3) side branch.

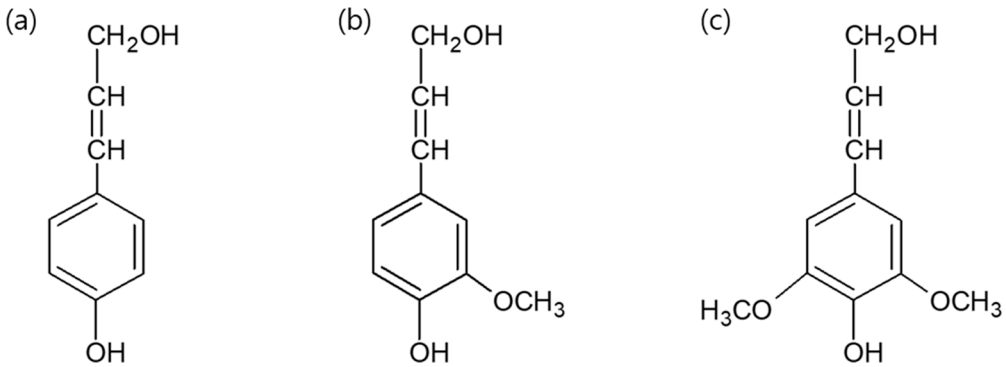


Figure 3. Basic lignin units: (**a**) p-counmaryl, (**b**) coniferyl, and (**c**) sinapyl alcohols.

However, not all chemical compositions are solely based on these chemical structures. In most cases, other elements such as nitrogen, sulfur, and chlorine are included in addition to C, H, and O. If these elements are considered only from the elemental composition perspective, an elemental analysis will divide only the organic components of the sample into C, H, N, and S, assuming the remaining mass to be oxygen, leading to misunderstandings regarding the composition of sulfur, chlorine, ash, and other elements present in the sample [4]. However, in proximate analysis, the total biomass composition can be determined [5]. Cellulose is primarily composed of volatile matter. Hemicellulose has less volatile matter and more fixed carbon than cellulose and includes some ash. Lignin has

relatively less volatile matter and more fixed carbon, with a particularly higher ash content than the other two components [6–9]. These characteristics cannot be determined using elemental analysis alone.

The ratios of these components vary depending on the biomass sources, such as herbaceous plants, hardwoods, or softwood. The TAPPI (Technical Association of the Pulp and Paper Industry) and the NREL (National Renewable Energy Laboratory) methods were used to determine the amounts of these three chemical components [10–15]. However, this method requires extensive time, samples, and equipment, such as HPLC and spectrometers. Consequently, various studies attempted alternative analyses for predicting biomass compositions rather than using conventional methods. Sheng et al. attempted to predict cellulose and lignin contents based on carbon dioxide and hydrogen consumption, and volatile matter [16]. Burhenne et al. predicted the chemical structure using elemental ratios [17]. However, the methods of Sheng et al. had a limited range of O/C and H/C, and that of Burhenne et al. was sensitive to even minor changes in the elemental composition. Díez et al. suggested the low-cost and rapid TGA-PKM method for determining the main lignocellulosic fraction contents of different types of biomasses from agricultural by-products [18]. Xing et al. reported a chemical constituent prediction model from ultimate analysis using a random forest model [19]. However, although an analysis of untreated biomass has been conducted, there is little research on the prediction of torrefied biomass. Therefore, this study proposed a model that predicts the cellulose, hemicellulose, and lignin contents based on the elemental content ratios determined during biofuel evaluation. From untreated biomass to torrefied biomass, this study attempted to make predictions using this method.

2. Methodology

2.1. Collection of Data

The elemental analysis, proximate analysis, and chemical structure results of the biomass were obtained from previous studies. A total of 174 data points were collected and normalized [20–56]. The collected data are summarized in Figure 4 and Table S1.

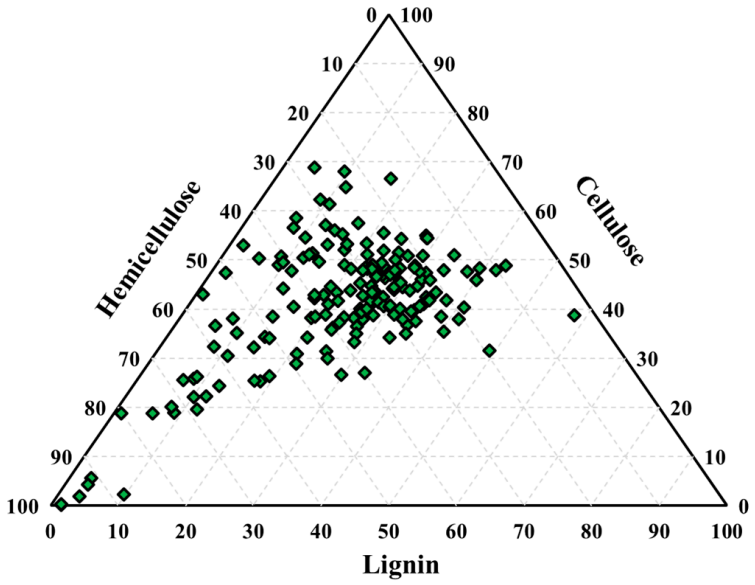


Figure 4. Distribution of the collected data according to chemical structure. Each square means the biomass composition of hemicellulos, cellulose and lignin.

2.2. Pearson Correlation Coefficient

The Pearson correlation coefficient (Equation (1)) was used to examine the correlation between the various elements (C, H, N, O, and S), and proximate (VM and FC) and

composition (Cell, Hemi, and Lig) analysis results. The Pearson correlation coefficient, as described in Equation (1), was used to analyze the degree of correlation between two populations. It ranges from −1 to 1, where positive and negative values indicate a proportional and inverse relationship, respectively. Values closer to −1 or 1 indicate a stronger linear correlation, whereas those closer to 0 indicate a weaker correlation [57]. Correlation equations with different goodness of fit values were obtained by performing linear and nonlinear regressions on the final analysis data using IBM SPSS version 22.0. The data analyses in this study utilized a combination of the "stepwise" and "enter" methods in SPSS software.

$$R = \frac{\left(\sum_{i=1}^{n}\left(X_i - \overline{X}\right)\left(Y_i - \overline{Y}\right)\right)}{\sqrt{\sum_{i=1}^{n}\left(X_i - \overline{X}\right)^2}\sqrt{\sum_{i=1}^{n}\left(Y_i - \overline{Y}\right)^2}} \quad (1)$$

2.2.1. Linear Regression

Linear regression is a statistical method commonly used to determine the value of a dependent variable based on that of an independent variable [58]. This technique uses a mathematical equation that outputs a simple value based on a combination of input properties. The linear regression equation is as follows [59]:

$$\hat{y} = \beta_O + x_1\beta_1 + x_2\beta_2 + x_3\beta_3 + \ldots + x_n\beta_n \quad (2)$$

2.2.2. Polynomial Regression

In polynomial regression, the data are approximated using a polynomial function [60]. It involves the use of high-order terms of variables for estimating the polynomial regression and creating a curved response surface [61]. Since there is no universal polynomial equation, the equation should be determined based on the specific problem at hand. The general expression for a polynomial of a function is as follows [59]:

$$f(x) = c_o + c_1x + c_2x^2 + \ldots + c_nx^n \quad (3)$$

2.3. Model Evaluation

Four performance metrics (equations) were used to evaluate the suitability of the models including the coefficient of determination (R^2), mean absolute error (*MAE*), root mean squared error (RMSE), and average absolute error (*AAE*). The coefficient of determination is a convenient tool for comparing relative performance. The *MAE* was used because it has the same units as the measured and predicted values and is intuitive. Although the RMSE had the advantage of reducing the distortion of values resulting from the square of the error, errors < 1 were further reduced due to the square, whereas errors > 1 increased. AAE and ABE represent the average error of the correlation equation; if they have positive values, they are evaluated highly, whereas if they have negative values, they are evaluated as somewhat low. The optimal selected prediction models were cross-validated using the data summarized in Table 1.

$$R^2 = 1 - \frac{\sum_{i=1}^{n} Value_M - Value_P}{\sum_{i=1}^{n} Value_M - \overline{Value_P}} \quad (4)$$

$$MAE = \frac{\sum_{i=1}^{n}(Valule_M - Value_P)}{n} \quad (5)$$

$$AAE = \frac{1}{n}\sum_{i=1}^{n}\left|\frac{Value_P - Value_M}{Value_M}\right| \quad (6)$$

Table 1. Data for cross-validation.

	Element Analysis			Proximate Analysis			Composition Analysis			Ref
	C	**H**	**O**	**VM**	**FC**	**Ash**	**Cell**	**Hemi**	**Lig**	
Mixed waste wood	48.08	5.69	45.8	86.15	10.44	3.41	42.27	27.05	30.68	[62]
Torrefied mixed waste wood (200 °C)	51.76	5.34	42.47	83.03	10.6	6.36	42.78	26.71	30.51	
Torrefied mixed waste wood (250 °C)	52.46	5.55	41.46	74.24	18.82	6.94	46.32	18.07	35.61	
Oak waste wood	47.26	5.95	46.46	87.3	12.05	0.65	44.64	29.72	25.64	
Torrefied Oak waste wood (200 °C)	48.78	5.86	44.94	86.52	12.62	0.86	43.77	28.01	28.22	
Logging residue	47.72	6.26	45.6	82.18	16.07	1.75	49.94	21.12	28.94	[63]
pine wood	45.83	6.35	47.51	83.1	16.3	0.6	50	19.67	30.33	[64]
Rice husk	44.91	6.93	47.21	68.55	22.95	8.5	48.32	37.17	14.52	[65]
Corn cob	46.29	6.69	46.69	67.68	22.29	10.03	47.37	36.84	15.79	
Groundnut shell	47.51	6.32	45.64	69.69	21.11	9.2	55.06	23.6	21.35	
Pine chip	47.31	6.65	45.86	85.97	13.76	0.27	54.01	16.89	29.09	[66]
Torrefied pine chip (225 °C)	49.61	6.09	44.15	84.42	14.89	0.7	44.56	13.91	41.53	
Torrefied pine chip (250 °C)	51.73	5.89	42.24	82.51	17.24	0.25	44.32	7.33	48.34	
Logging residue chip	47.72	6.26	45.6	82.16	16.07	1.77	48.75	17.24	34.01	
Torrefied logging residue chip (225 °C)	50.51	6.14	43.05	80.73	17.9	1.37	46.11	16.59	37.30	
Torrefied logging residue chip (250 °C)	53.81	5.75	40.14	78.14	20.37	1.49	44.37	6.75	48.88	
Torrefied logging residue chip (275 °C)	53.75	5.44	40.5	71.43	26.69	1.88	37	5.68	57.32	
Loblolly pine	50.78	6.29	42.84	84.6	14.8	0.6	42.52	22.03	35.45	[67]
Torrefied loblolly pine (270 °C 2.5 min)	55.36	5.98	38.55	78.6	20.8	0.6	39.29	13.92	46.79	
Torrefied loblolly pine (300 °C 2.5 min)	57.74	5.83	36.28	76.4	22.8	0.8	35.85	10.22	53.93	
Torrefied loblolly pine (330 °C 2.5 min)	66.77	4.94	28.01	59.96	38.64	1.4	19.33	1.25	79.42	
Palm mesocarp fiber	46.29	4.67	47.37	63.29	29.49	7.22	30.43	29.25	40.32	[68]
Palm kernel shell	47.77	4.06	47.55	59.07	34.36	6.57	30.28	28.31	41.41	
Sugarcane bagasse sample	46.32	6.28	46.74	83.55	14.28	2.17	43.35	35.33	21.32	[69]
Torrefied sugarcane bagasse (200 °C)	41.88	4.21	53.59	71.26	26.97	1.77	44.19	12.35	43.46	
Torrefied sugarcane bagasse (225 °C)	47.1	4.72	47.79	71.95	25.55	2.49	34.03	15.39	50.58	
Torrefied sugarcane bagasse (250 °C)	52.63	3.79	43.16	62.27	34.5	3.22	25.82	8.29	65.89	

3. Results & Discussions

3.1. Result of Pearson Correlation Coefficient

The results of Pearson's correlation coefficient are summarized in Figure 5. Cellulose showed a negative correlation with *C*, but a positive correlation with *H* and *O*. Despite

the negative correlation between *C* and cellulose, both *H*/*C* and *O*/*C* showed positive correlations. In particular, the *H*/*C* ratio exhibited a strong positive correlation (0.658). The *VM* showed a positive correlation, whereas the *FC* showed a negative correlation. *FC*/*VM* showed a strong negative correlation, which was attributed to the low *FC* content of cellulose. The correlation between the *VM*/*FC* ratios was low. Hemicellulose showed a stronger negative correlation with C than cellulose. *H*, *O*, *H*/*C*, and *O*/*C* showed positive correlations, but there was a slight difference compared to their relationship with cellulose. The correlation between *H* and hemicellulose showed a weaker positive correlation (0.26) than that between cellulose and *H*. On the other hand, the correlation between *O* and hemicellulose was higher (0.42) than that between cellulose and *O* (0.30). As a result, there was a slight difference between the *H*/*C* and *O*/*C* ratios. In the case of lignin and each element, there were many cases in which their correlations were opposite to those of cellulose and hemicellulose. Lignin was positively correlated with C and negatively correlated with *H*, *O*, *H*/*C*, and *O*/*C*, which were positively correlated with cellulose and hemicellulose. Lignin levels showed a strong negative correlation with *VM* and a strong positive correlation with *FC*. These results were based on the fact that cellulose and hemicellulose are composed of linear carbon structures, whereas lignin has a ring structure that forms stronger bonds, making it less volatile. In addition, there was a strong positive correlation in the case of *FC*/*VM* due to its relationship with cellulose, such as *FC*. However, there was no strong correlation in the case of the *VM*/*FC*. Based on these results, the basic prediction model that was suggested is as follows:

$$Cell = f(C,\ H,\ O,\ VM,\ FC) \tag{7}$$

$$Hemi = g(C,\ H,\ O,\ VM,\ FC) \tag{8}$$

$$Lig = h(C,\ H,\ O,\ VM,\ FC) \tag{9}$$

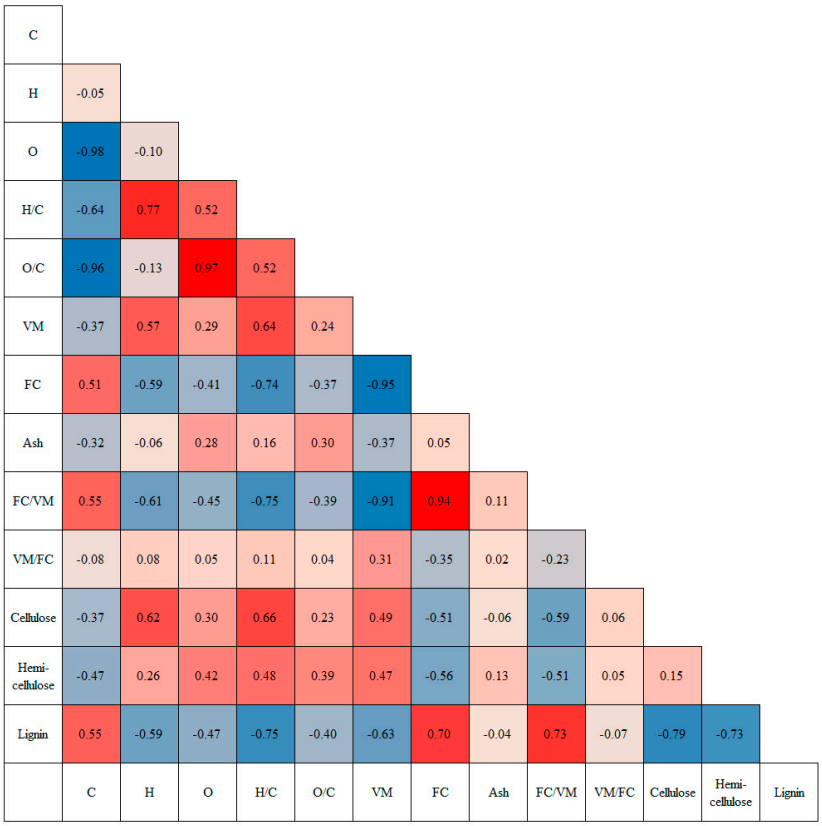


Figure 5. Result of Pearson correlation coefficient.

3.2. Prediction Model for Cellulose

The equations with the highest R^2_P for predicting cellulose content are summarized in Table 2. Differences were observed between C1 and C2 when the second-order terms C, H, O, and FC/VM were added to the equation. Due to the increase in the number of factors involved in the equation, C2 showed an increased R^2_P of 0.6342, whereas C1 had an R^2_P of 0.6104. Additionally, lower $RMSE_P$, MAE_P, and AAE_P values were observed. When comparing C2 and C3, the impact of the second-order terms on VM, FC, and FC/VM was considered. The R^2_P value for C3 increased slightly to 0.6362. However, the $RMSE_P$, MAE_P, and AAE_P increased for C3, with values of 7.3263, 5.8115, and 43.1320, respectively, compared with C2 values of 7.3013, 5.4302, and 32.7348. This indicates that C3 had larger errors, as shown in Figure 6. The red trend line in Figure 6 was used as a reference for significance at the level of 0.01. As expected, there was little difference in the trends between C2 and C3; however, some data points from C3 deviated further from the trend line compared to those from C2.

Table 2. Results of predicted model for cellulose.

No.	Proposed Models	R^2_P [-]	$RMSE_P$ [%]	MAE_P [%]	AAE_P [%]
C1	$Cell = -152.237 + 0.838C - 10.405H + 3.3091O - 37.061\left(\frac{H}{C}\right)^2 + 177.211\left(\frac{H}{C}\right) + 20.086\left(\frac{O}{C}\right)^2 - 136.126\left(\frac{O}{C}\right) + 0.151VM + 0.391FC - 4.52\left(\frac{FC}{VM}\right)$	0.6104	7.3666	5.6839	49.2202
C2	$Cell = 678.363 + 0.270C^2 - 0.632H^2 - 0.166O^2 - 34.026C + 24.548H + 22.108O - 15.474\left(\frac{H}{C}\right)^2 - 10.580\left(\frac{H}{C}\right) + 94.988\left(\frac{O}{C}\right)^2 - 510.643\left(\frac{O}{C}\right) + 0.250VM + 0.290FC - 3.866\left(\frac{FC}{VM}\right)^2 + 10.266\left(\frac{FC}{VM}\right)$	0.6342	7.3013	5.4302	32.7348
C3	$Cell = 810.611 + 0.311C^2 - 0.657H^2 - 0.165O^2 - 39.014C + 23.282H + 23.513O - 14.962\left(\frac{H}{C}\right)^2 - 4.252\left(\frac{H}{C}\right) + 104.943\left(\frac{O}{C}\right)^2 - 595.105\left(\frac{O}{C}\right) - 0.001VM^2 + 0.551VM - 0.012FC^2 + 0.116FC - 12.486\left(\frac{FC}{VM}\right)^2 + 59.697\left(\frac{FC}{VM}\right)$	0.6362	7.3263	5.8115	43.1320

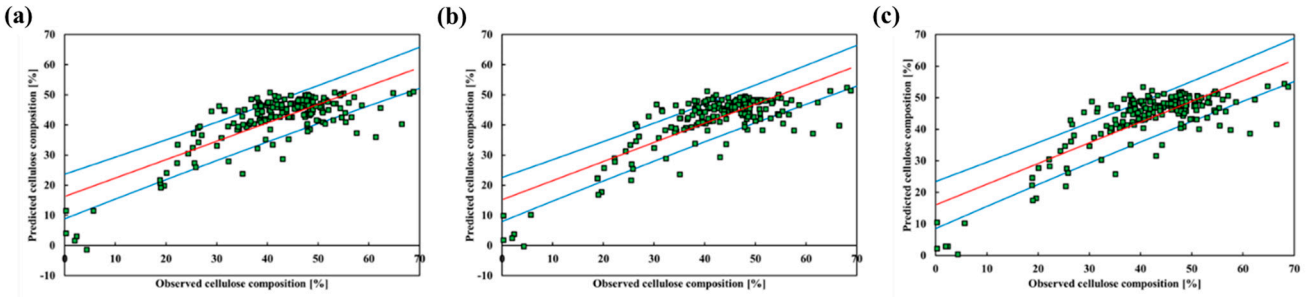


Figure 6. Prediction results plotted using linear regression for cellulose: (**a**) C1; (**b**) C2; (**c**) C3. Green square means predicted and measured cellulose composition of biomass. Blue line means 99% confidence interval and red line means trend line.

3.3. Prediction Model for Hemicellulose

Various factors were added to predict the hemicellulose content. However, the R^2_P of the model was lower than that of cellulose and lignin. The equations with the highest prediction accuracies are listed in Table 3. When comparing H1 and H2, adding factors

related to FC/VM resulted in a higher R^2_P value than adding the square terms C, H, and O. This suggested that the relationship between hemicellulose and FC/VM has a stronger correlation than that with C, H, and O, based on the Pearson correlation coefficients. The R^2_P values for H1 and H2 were 0.4901 and 0.4803, respectively, showing no significant differences. However, H1 exhibited a slightly higher trend. Additionally, the MAE_P for H2 was lower (5.6556) than that for H1 (6.1396). When comparing H1 and H3, there was a difference when considering the squared terms of C, H, and O. H3 showed a higher R^2_P (0.5112) than H1, but the $RMSE_P$ was higher for H3 (7.7173) compared to H1 (7.4899). However, MAE_P and AAE_P were lower for H3 (5.7038 and 48.7658, respectively). The results for each prediction equation are presented in Figure 7. The red line represents the trend line, and the blue line is the confidence interval with a 0.01 significance level. The lowest overshoot was observed for H2. For H1 and H2, relatively significant deviations from the trend line were observed in the prediction results, which contributed to the higher RMSE values.

Table 3. Results of predicted model for hemicellulose.

No.	Proposed Models	R^2_P [-]	$RMSE_P$ [%]	MAE_P [%]	AAE_P [%]
H1	$Hemi = 398.274 - 0.118C - 36.749H + 3.886O - 51.759\left(\frac{H}{C}\right)^2 + 300.624\left(\frac{H}{C}\right) + 48.091\left(\frac{O}{C}\right)^2 - 286.902\left(\frac{O}{C}\right) + 0.055VM^2 - 0.003FC^2 - 9.205VM + 3.077FC + 50.49\left(\frac{FC}{VM}\right)^2 - 275.401\left(\frac{FC}{VM}\right)$	0.4901	7.4899	6.1396	53.1694
H2	$Hemi = 1465.909 + 0.212C^2 + 0.66H^2 + 0.101O^2 - 33.374C - 49.249H + 10.983O - 66.583\left(\frac{H}{C}\right)^2 + 363.635\left(\frac{H}{C}\right) + 209.649\left(\frac{O}{C}\right)^2 - 1329.208\left(\frac{O}{C}\right) - 0.376VM - 0.673FC$	0.4803	7.5634	5.6556	45.8770
H3	$Hemi = 1481.552 + 0.152C^2 + 1.823H^2 + 0.093O^2 - 24.536C - 75.775H + 9.712O - 94.539\left(\frac{H}{C}\right)^2 + 494.635\left(\frac{H}{C}\right) + 195.349\left(\frac{O}{C}\right)^2 - 1215.865\left(\frac{O}{C}\right) + 0.052VM^2 - 8.651VM - 0.008FC^2 + 2.644FC + 42.716\left(\frac{FC}{VM}\right)^2 - 231.488\left(\frac{FC}{VM}\right)$	0.5112	7.7173	5.7038	48.7658

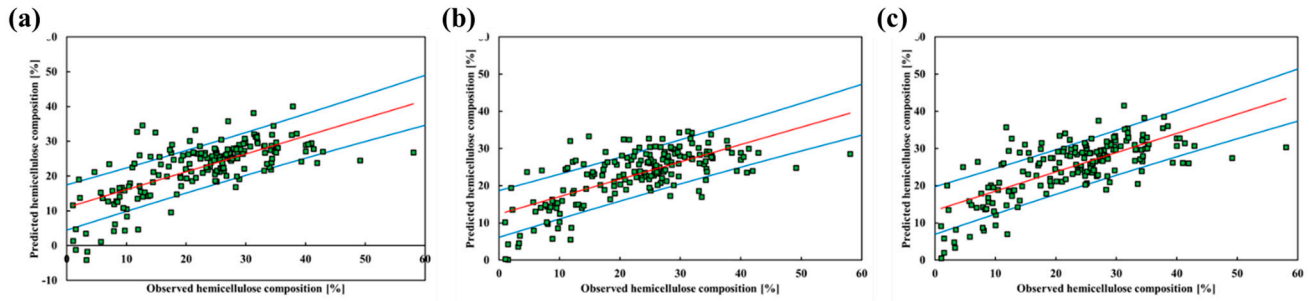


Figure 7. Prediction results plotted using linear regression for hemicellulose: (**a**) H1; (**b**) H2; (**c**) H3. Green square means predicted and measured hemicellulose composition of biomass. Blue line means 99% confidence interval and red line means trend line.

3.4. Prediction Model for Lignin

The optimal lignin contents are listed in Table 4. Lignin exhibited higher R^2_P values than cellulose and hemicellulose. In the case of L1, the least number of factors was con-

sidered. However, the R^2_P value was 0.7247, which was higher than that observed for cellulose and hemicellulose. L1 and L2 were determined based on whether the second-order VM and FC were considered. L2, which was considered the second-order VM and FC, showed a higher R^2_P (0.7348). However, the $RMSE_P$, MAE_P, and AAE_P were lower for L1. L3 exhibited the highest R^2_P value (0.7914). The $RMSE_P$, MAE_P, and AAE_P were also lower, with values of 7.9857, 5.9868, and 26.3036, respectively. As shown in Figure 8, which graphically represents the results, L1 and L2 exhibited excessive predictions when the observed values were between 90 and 100%. However, for L3, excessive predictions were not observed, although the confidence interval was exceeded.

Table 4. Results of predicted model for lignin.

No.	Proposed Models	R^2_P [-]	$RMSE_P$ [%]	MAE_P [%]	AAE_P [%]
L1	$Lig = 165.252 + 40.196\left(\frac{H}{C}\right)^2 - 130.961\left(\frac{H}{C}\right) + 21.354\left(\frac{O}{C}\right)^2 - 50.265\left(\frac{O}{C}\right) - 0.11VM + 0.164FC - 4.561\left(\frac{FC}{VM}\right)$	0.7247	9.0426	7.0424	28.6080
L2	$Lig = -121.824 + 39.757\left(\frac{H}{C}\right)^2 - 128.192\left(\frac{H}{C}\right) + 23.719\left(\frac{O}{C}\right)^2 - 56.877\left(\frac{O}{C}\right) - 0.042VM^2 + 6.932VM + 0.000473FC^2 - 2.954FC - 45.172\left(\frac{FC}{VM}\right)^2 + 239.132\left(\frac{FC}{VM}\right)$	0.7348	9.1532	7.1781	31.1764
L3	$Lig = -2192.163 - 0.463C^2 - 1.165H^2 + 0.072O^2 + 63.550C + 52.493H - 33.225O + 109.501\left(\frac{H}{C}\right)^2 - 490.382\left(\frac{H}{C}\right) - 300.292\left(\frac{O}{C}\right)^2 + 180.969\left(\frac{O}{C}\right) - 0.050VM^2 + 8.100VM + 0.020FC^2 - 2.760FC - 30.230\left(\frac{FC}{VM}\right)^2 + 171.791\left(\frac{FC}{VM}\right)$	0.7914	7.9857	5.9868	26.3036

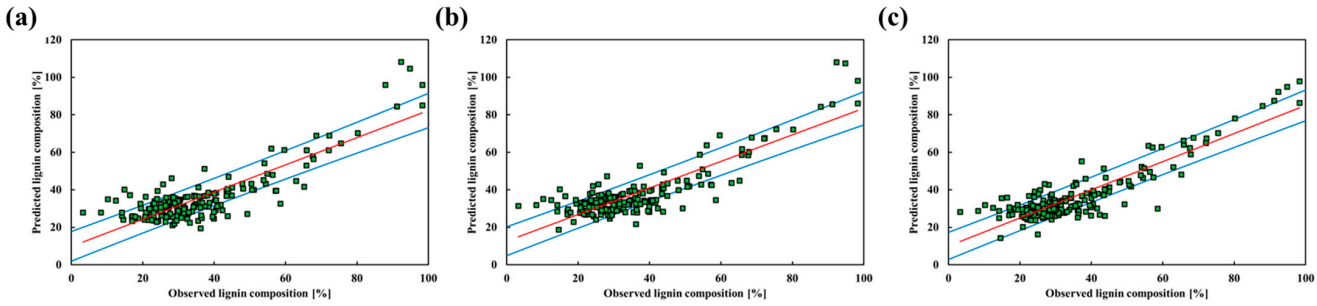


Figure 8. Prediction results plotted using linear regression for lignin: (**a**) L1; (**b**) L2; (**c**) L3. Green square means predicted and measured lignin composition of biomass. Blue line means 99% confidence interval and red line means trend line.

3.5. Cross-Validation Results for Cellulose

The cross-validation results for the cellulose prediction are presented in Table 5 and Figure 9. R^2_{CV} was higher than R^2_P. The R^2_P values for C1, C2, and C3 were 0.6104, 0.6342, and 0.6362, respectively. The R^2_{CV} values were 0.7837, 0.7428, and 0.7387, respectively. In particular, C1, which had the lowest R^2_P value, also had the highest R^2_{CV} value. The $RMSE_{CV}$ for C1 is 3.8149. Based on the validation results, C1 was identified as the optimal prediction equation.

Table 5. Cross-validation results of the predicted model using linear regression and algorithm for cellulose.

	R^2_{CV} [-]	$RMSE_{CV}$ [%]	MAE_{CV} [%]	AAE_{CV} [%]
C1	0.7837	3.8149	3.0291	7.5647
C2	0.7458	4.3132	3.2023	7.7781
C3	0.7387	4.8125	4.1379	6.9634

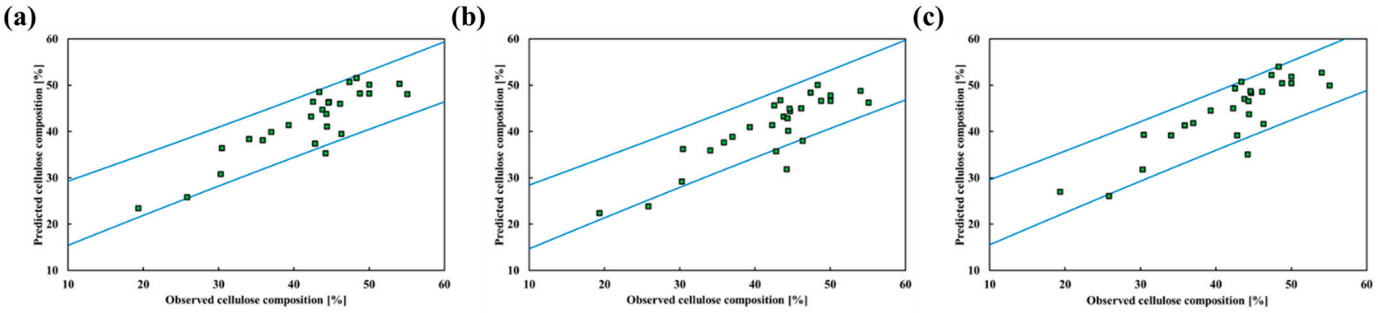


Figure 9. Cross-validation results of the predicted model plotted using linear regression for cellulose: (**a**) C1; (**b**) C2; (**c**) C3. Green square means predicted and measured cellulose composition of biomass. Blue line means 99% confidence interval.

3.6. Cross-Validation Results for Hemicellulose

The cross-validation results for hemicellulose prediction showed lower performance than that of the prediction model. The results are summarized in Table 6. The R^2_P values for H1, H2, and H3 were approximately 0.5, with values of 0.4901, 0.4803, and 0.5112, respectively. However, the R^2_{CV} values were lower at 0.3292, 0.4004, and 0.3280 for H1, H2, and H3, respectively. This low performance was also reflected in the $RMSE_{CV}$ values, which ranged from 8.2683 to 9.8534. The validation results are illustrated in Figure 10, which shows that they fall within the 99% confidence interval. In Figure 10a,b, the results are skewed towards the upper end of the confidence interval. Thus, H2 was selected as the optimal concentration.

Table 6. Cross-validation results of the predicted model using linear regression and algorithm for hemicellulose.

	R^2_{CV} [-]	$RMSE_{CV}$ [%]	MAE_{CV} [%]	AAE_{CV} [%]
H1	0.3292	8.6098	7.2671	61.0694
H2	0.4004	8.2683	7.2084	66.4448
H3	0.3280	9.8534	8.7032	66.0180

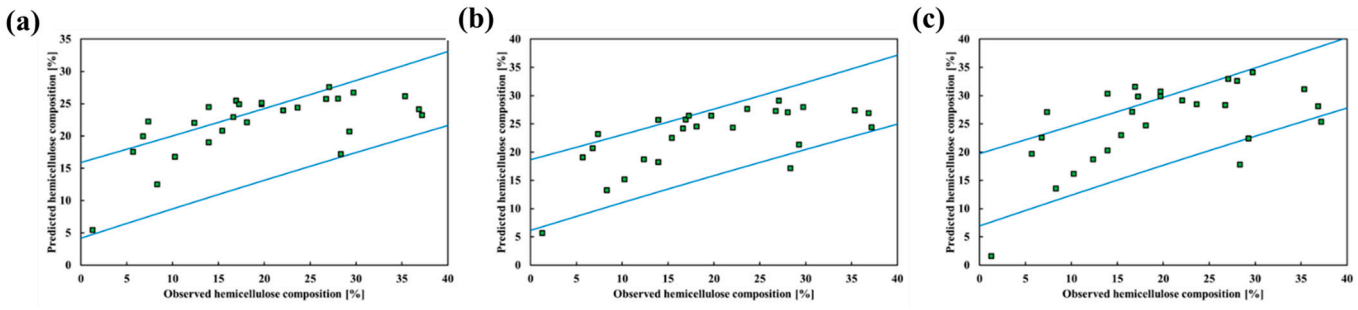


Figure 10. Cross-validation results of the predicted model plotted using linear regression and algorithm for hemicellulose: (**a**) H1; (**b**) H2; (**c**) H3. Green square means predicted and measured hemicellulose composition of biomass. Blue line means 99% confidence interval.

3.7. Cross-Validation Results for Lignin

Similar to R^2_P, lignin exhibited a higher R^2_{CV} compared to cellulose and hemicellulose. The results are summarized in Table 7 and Figure 11. The R^2_P values for L1, L2, and L3 were 0.7247, 0.7348, and 0.7914, respectively, The corresponding R^2_{CV} values are 0.7728, 0.7757, and 0.7427, respectively. The R^2_{CV} for L3 was lower than its R^2_P but increased in L1 and L2. The $RMSE_{CV}$ values ranged from 7.2735 to 7.7483. Based on the validation results, L2 was considered optimal.

Table 7. Cross-validation results of the predicted model using linear regression and algorithm for lignin.

	R^2_{CV} [-]	$RMSE_{CV}$ [%]	MAE_{CV} [%]	AAE_{CV} [%]
L1	0.7728	7.7483	6.7726	19.8385
L2	0.7757	7.2735	6.3054	20.2150
L3	0.7427	7.7133	6.6112	19.7636

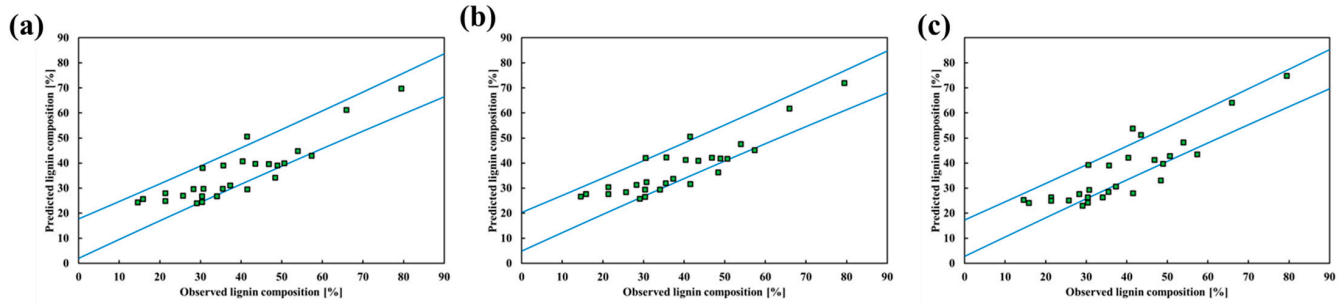


Figure 11. Cross-validation results of the predicted model plotted using linear regression and algorithm for lignin: (**a**) L1; (**b**) L2; (**c**) L3. Green square means predicted and measured lignin composition of biomass. Blue line means 99% confidence interval.

3.8. Prediction and Cross-Validation of Hemicellulose Using Cellulose and Lignin

Based on the relatively stronger correlation between lignin and cellulose than with hemicellulose, the decision was made to predict hemicellulose content based on lignin and cellulose using the selected optimal conditions of C1 and L2. The results are summarized in Table 8 and Figure 12. The prediction results showed an R^2_P value of 0.3770, which was lower than that of the hemicellulose prediction for H1, H2, and H3. Consequently, the $RMSE_P$, MAE_P, and AAE_P were higher, with values of 8.5612, 6.7581, and 50.3295, respectively, compared with the results of the previous prediction equations. In Figure 12a, there were cases where the hemicellulose contents were negative, which was attributed

to the overprediction of the cellulose and lignin contents. The CV results differed from the predicted results. The R^2_{CV} showed a higher value (0.4292) than the R^2_{CV} of the other prediction equations. Similarly, the $RMSE_{CV}$ was lower (7.5979) when C1 and L2 were used for prediction compared to H1, H2, and H3, which had values ranging from 8.2683 to 9.8534. Based on these results, it was determined that using H2 or predicting hemicellulose based on cellulose and lignin yielded optimal predictions.

Table 8. Prediction and cross-validation results of hemicellulose based on C1 and L1.

R^2_P [-]	$RMSE_P$ [%]	MAE_P [%]	AAE_P [%]	R^2_{CV} [-]	$RMSE_{CV}$ [%]	MAE_{CV} [%]	AAE_{CV} [%]
0.3770	8.5612	6.7581	50.3295	0.4292	7.5979	6.3346	51.9966

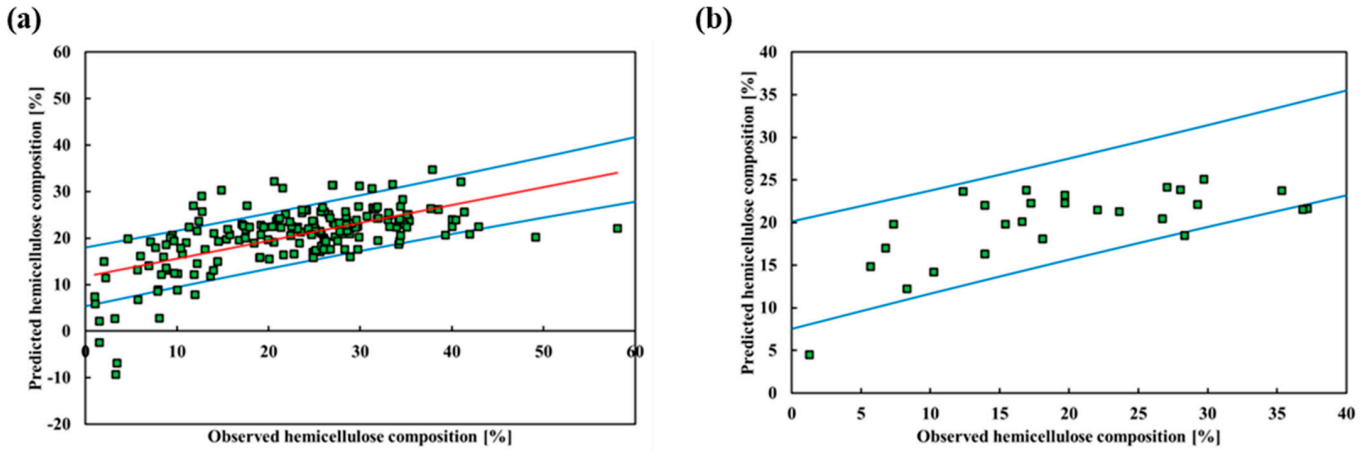


Figure 12. Hemicellulose prediction results: (**a**) cross-validation results; (**b**) results plotted using C1 and L2. Green square means predicted and measured hemicellulose composition of biomass. Blue line means 99% confidence interval and red line means trend line.

3.9. Application Performance

To thoroughly assess the performance of the developed models, the models are utilized to make predictions on the chemical constituents of the application database. It is important to note that all the samples in this database are different from those present in the training database. Since the mass fraction of volatile matter is provided in the application database, it is possible to directly compare the currently developed model with the previous correlation proposed by Sheng and Azevedo [70]. These correlations can be expressed using the following equations:

$$Cellulose = -1019.07 + 293.810\left(\frac{O}{C}\right) - 187.639\left(\frac{O}{C}\right)^2 + 65.1426\left(\frac{H}{C}\right) - 19.3025\left(\frac{H}{C}\right)^2 + 21.7448VM - 0.132123VM^2 \quad (10)$$

$$lignin = 612.099 + 195.366\left(\frac{O}{C}\right) - 156.535\left(\frac{O}{C}\right)^2 + 511.357\left(\frac{H}{C}\right) - 177.025\left(\frac{H}{C}\right)^2 + 21.7448VM + 0.145306VM^2 \quad (11)$$

According to Sheng and Azevedo (2002), the correlation they developed was based on samples with the following ranges of parameters: O/C ratio: 0.56 to 0.83, H/C ratio: 1.26 to 1.69, and volatile matter (VM): 73% to 86%. These ranges were used to establish the correlation between the mass fraction of the volatile matter and other chemical constituents in their model. Figure 13 shows the direct comparison of the chemical composition predicted with the present model and the correlation developed by Sheng and Azevedo. Figure 13 also illustrates the direct comparisons of the chemical composition predicted

using the current model, the previous correlation proposed by Sheng and Azevedo, and the experimental data. In the figure, the green lines represent the data distribution, where the relative error is ±20%. This provided a visual representation of the agreement between the predicted values and the experimental data for each model. In the case of Sheng and Azevedo's model, the prediction performance for torrefied samples was low. Values in the ranges of −422.80–−5.20%, −225.21–144.62%, and −39.32–8731.05% were obtained for cellulose, hemicellulose, and lignin, respectively. The models in this study showed −19.96–21.59%, −24.77–84.08%, and −39.23–355.61%, respectively.

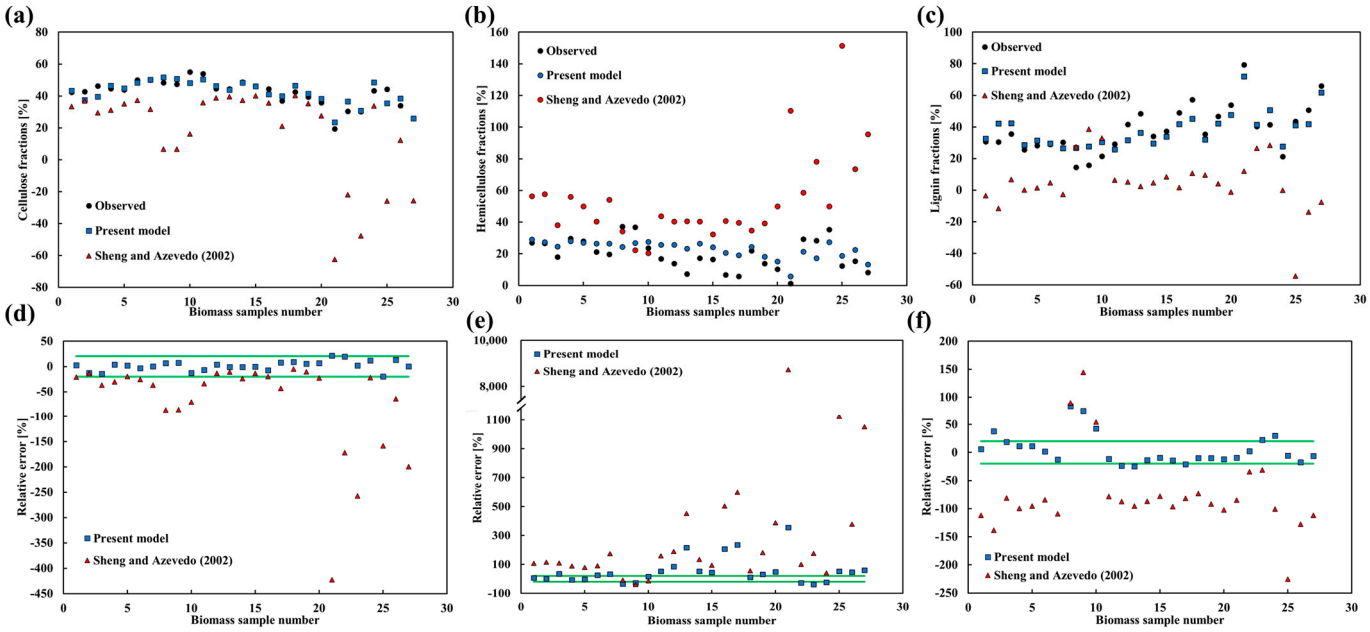


Figure 13. Comparison of the chemical composition predicted using the correlation developed by Sheng and Azevdo and the composition predicted using the present models with the data for the application database: (**a**) cellulose fractions; (**b**) hemicellulose fractions; (**c**) lignin fractions; (**d**) cellulose relative error; (**e**) hemicellulose relative error; (**f**) lignin relative error. Green line indicates relative ±20% [16].

4. Conclusions

This study aimed to predict the cellulose, hemicellulose, and lignin contents based on elemental and industrial analyses, instead of using conventional methods such as HPLC or infrared spectroscopy. Herein, various models were proposed to obtain regression prediction equations using linear regression. The R^2_P values for cellulose, hemicellulose, and lignin using linear regression were between 0.6104 and 0.6362, 0.4803 and 0.5112, and 0.7247 and 0.7914, respectively. Prediction for hemicellulose exhibited the lowest performance. Based on this, the optimal equation was used for cross-validating the same. The optimal conditions for cellulose and lignin were selected as C1 and L2 due to their highest R^2_{CV} and lowest $RMSE_{CV}$, MAE_{CV}, and AAE_{CV}. To address the low accuracy of the hemicellulose prediction model, it was predicted based on the cellulose and lignin prediction models, which were validated as optimal. Despite the lower R^2 and higher RMSE values compared to those of the hemicellulose prediction equations, the cross-validation results were higher than those of the other prediction equations. Despite the lower performance in terms of R^2 and higher RMSE compared to those of lignin and cellulose, the prediction and cross-validation results were deemed optimal when both prediction and cross-validation results were considered. Therefore, using both cellulose and lignin for the prediction and the H2 equation was deemed to be the optimal approach.

This study had some limitations. Although we considered data from a wide range of samples, including torrefied samples, predictions were only made using data for woody

and herbaceous biomasses. Therefore, the predictions may be inaccurate for food waste or sewage sludge. In the case of hemicellulose, low prediction accuracy was observed due to its low content compared to cellulose and lignin. In addition, it was shown to represent a low prediction due to a decrease in various ranges, depending on the process conditions. Therefore, future research should provide models for a wider range of biomasses and improve prediction equations based on more data pertaining to woody and herbaceous biomass.

Supplementary Materials: The following supporting information can be downloaded at: https://www.mdpi.com/article/10.3390/en16145341/s1, Table S1: Data for model prediction. Reference [70] is cited in supplementary materals.

Author Contributions: Conceptualization, S.Y.P., S.J.K., K.C.O. and D.K.; methodology, S.Y.P. and K.C.O.; validation, S.Y.P. and K.C.O.; investigation, S.Y.P., K.C.O., Y.K.J. and L.H.C.; formal analysis, S.Y.P., S.J.K. and K.C.O.; writing—original draft, S.Y.P. and D.K.; writing—review and editing, S.Y.P., K.C.O. and D.K.; data curation, S.Y.P. and K.C.O.; writing—review and editing, D.K.; supervision, D.K. All authors have read and agreed to the published version of the manuscript.

Funding: This study was conducted with the support of the R&D Program for Forest Science Technology (Project No. "FTIS 2021352B10-2223-AC03") provided by the Korea Forest Service (Korea Forestry Promotion Institute) and supported by the Korea Institute of Planning and Evaluation for Technology in Food, Agriculture and Forestry (IPET) through the Agriculture, Food and Rural Affairs Convergence Technologies Program for Educating Creative Global Leader, funded by the Ministry of Agriculture, Food and Rural Affairs (MAFRA) (Project No. 320001-4), Republic of Korea.

Data Availability Statement: The data used to support the findings of this study are included within the article.

Conflicts of Interest: The authors declare no conflict of interest.

References

1. O'sullivan, A.C. Cellulose: The Structure Slowly Unravels. *Cellulose* **1997**, *4*, 173–207. [CrossRef]
2. Rao, J.; Lv, Z.; Chen, G.; Peng, F. Hemicellulose: Structure, Chemical Modification, and Application. *Prog. Polym. Sci.* **2023**, *140*, 101675. [CrossRef]
3. Li, M.; Pu, Y.; Ragauskas, A.J. Current Understanding of the Correlation of Lignin Structure with Biomass Recalcitrance. *Front. Chem.* **2016**, *4*, 45. [CrossRef] [PubMed]
4. Smoot, L.D.; Baxter, L.L. Fossil Fuel Power Stations—Coal Utilization. In *Encyclopedia of Physical Science and Technology*, 3rd ed.; Meyers, R.A., Ed.; Academic Press: New York, NY, USA, 2003; pp. 121–144. ISBN 9780122274107.
5. Basu, P. Chapter 13—Analytical Techniques. In *Biomass Gasification, Pyrolysis and Torrefaction: Practical Design and Theory*; Basu, P., Ed.; Biomass Gasification, Pyrolysis and Torrefaction (Second Edition); Academic Press: Boston, MA, USA, 2013; pp. 439–455. ISBN 9780123964885.
6. Ozbayoglu, G. 3.19 Energy Production From Coal. In *Comprehensive Energy Systems*; Dincer, I., Ed.; Elsevier: Oxford, UK, 2018; pp. 788–821. ISBN 9780128149256.
7. Qu, T.; Guo, W.; Shen, L.; Xiao, J.; Zhao, K. Experimental Study of Biomass Pyrolysis Based on Three Major Components: Hemicellulose, Cellulose, and Lignin. *Ind. Eng. Chem. Res.* **2011**, *50*, 10424–10433. [CrossRef]
8. Zhao, C.; Jiang, E.; Chen, A. Volatile Production from Pyrolysis of Cellulose, Hemicellulose and Lignin. *J. Energy Inst.* **2017**, *90*, 902–913. [CrossRef]
9. Kim, D.; Lee, K.; Park, K.Y. Upgrading the Characteristics of Biochar from Cellulose, Lignin, and Xylan for Solid Biofuel Production from Biomass by Hydrothermal Carbonization. *J. Ind. Eng. Chem.* **2016**, *42*, 95–100. [CrossRef]
10. Technical Association of the Pulp and Paper Industry (TAPPI). Solvent Extractives of Wood and Pulp, Test Method T 204 Cm-97. 2007. Available online: https://www.astm.org/d1106-96r01.html (accessed on 1 July 2023).
11. Technical Association of the Pulp and Paper Industry (TAPPI). Standard Test Method for Acid-Insoluble Lignin in Wood. 2007.
12. Technical Association of the Pulp and Paper Industry (TAPPI). Alpha-, Beta- and Gamma-Cellulose in Pulp, Test Method T 203 Cm-22. 1999. Available online: https://imisrise.tappi.org/TAPPI/Products/01/T/0104T203.aspx (accessed on 1 July 2023).
13. Sluiter, A.; Ruiz, R.; Scarlata, C.; Sluiter, J.; Templeton, D. *Determination of Extractives in Biomass: Laboratory Analytical Procedure (LAP)*; National Renewable Energy Laboratory: Golden, CO, USA, 2008.
14. Sluiter, A.; Hames, B.; Ruiz, R.; Scarlata, C.; Sluiter, J.; Templeton, D. *Determination of Ash in Biomass: Laboratory Analytical Procedure (LAP)*; National Renewable Energy Laboratory: Golden, CO, USA, 2008.

15. Sluiter, A.; Hames, B.; Ruiz, R.; Scarlata, C.; Sluiter, J.; Templeton, D.; Crocker, D. *Determination of Structural Carbohydrates and Lignin in Biomass: Laboratory Analytical Procedure (LAP)*; National Renewable Energy Laboratory: Golden, CO, USA, 2008.
16. Sheng, C.; Azevedo, J.L.T. Modeling Biomass Devolatilization Using the Chemical Percolation Devolatilization Model for the Main Components. *Proc. Combust. Inst.* **2002**, *29*, 407–414. [CrossRef]
17. Burhenne, L.; Messmer, J.; Aicher, T.; Laborie, M.P. The Effect of the Biomass Components Lignin, Cellulose and Hemicellulose on TGA and Fixed Bed Pyrolysis. *J. Anal. Appl. Pyrolysis* **2013**, *101*, 177–184. [CrossRef]
18. Díez, D.; Urueña, A.; Piñero, R.; Barrio, A.; Tamminen, T. Determination of Hemicellulose, Cellulose, and Lignin Content in Different Types of Biomasses by Thermogravimetric Analysis and Pseudocomponent Kinetic Model (TGA-PKM Method). *Processes* **2020**, *8*, 1048. [CrossRef]
19. Xing, J.; Luo, K.; Wang, H.; Fan, J. Estimating Biomass Major Chemical Constituents from Ultimate Analysis Using a Random Forest Model. *Bioresour. Technol.* **2019**, *288*, 121541. [CrossRef]
20. Peng, J.; Bi, X.T.; Lim, J.; Sokhansanj, S. Development of Torrefaction Kinetics for British Columbia Softwoods. *Int. J. Chem. React. Eng.* **2012**, *10*, 1–40. [CrossRef]
21. Chen, W.H.; Kuo, P.C. A Study on Torrefaction of Various Biomass Materials and Its Impact on Lignocellulosic Structure Simulated by a Thermogravimetry. *Energy* **2010**, *35*, 2580–2586. [CrossRef]
22. Rousset, P.; Aguiar, C.; Labbé, N.; Commandré, J.M. Enhancing the Combustible Properties of Bamboo by Torrefaction. *Bioresour. Technol.* **2011**, *102*, 8225–8231. [CrossRef]
23. Granados, D.A.; Ruiz, R.A.; Vega, L.Y.; Chejne, F. Study of Reactivity Reduction in Sugarcane Bagasse as Consequence of a Torrefaction Process. *Energy* **2017**, *139*, 818–827. [CrossRef]
24. Cahyanti, M.N.; Doddapaneni, T.R.K.C.; Madissoo, M.; Pärn, L.; Virro, I.; Kikas, T. Torrefaction of Agricultural and Wood Waste: Comparative Analysis of Selected Fuel Characteristics. *Energies* **2021**, *14*, 2774. [CrossRef]
25. Chen, W.H.; Hsu, H.C.; Lu, K.M.; Lee, W.J.; Lin, T.C. Thermal Pretreatment of Wood (Lauan) Block by Torrefaction and Its Influence on the Properties of the Biomass. *Energy* **2011**, *36*, 3012–3021. [CrossRef]
26. Chen, W.H.; Cheng, W.Y.; Lu, K.M.; Huang, Y.P. An Evaluation on Improvement of Pulverized Biomass Property for Solid Fuel through Torrefaction. *Appl. Energy* **2011**, *88*, 3636–3644. [CrossRef]
27. Ma, Z.; Zhang, Y.; Shen, Y.; Wang, J.; Yang, Y.; Zhang, W.; Wang, S. Oxygen Migration Characteristics during Bamboo Torrefaction Process Based on the Properties of Torrefied Solid, Gaseous, and Liquid Products. *Biomas. Bioenergy* **2019**, *128*, 105300. [CrossRef]
28. Kanwal, S.; Chaudhry, N.; Munir, S.; Sana, H. Effect of Torrefaction Conditions on the Physicochemical Characterization of Agricultural Waste (Sugarcane Bagasse). *Waste Manag.* **2019**, *88*, 280–290. [CrossRef]
29. Jiang, H.; Ye, Y.; Lu, P.; Zhao, M.; Xu, G.; Chen, D.; Song, T. Effects of Torrefaction Conditions on the Hygroscopicity of Biochars. *J. Energy Inst.* **2021**, *96*, 260–268. [CrossRef]
30. Li, M.F.; Chen, C.Z.; Li, X.; Shen, Y.; Bian, J.; Sun, R.C. Torrefaction of Bamboo under Nitrogen Atmosphere: Influence of Temperature and Time on the Structure and Properties of the Solid Product. *Fuel* **2015**, *161*, 193–196. [CrossRef]
31. Rodriguez Alonso, E.; Dupont, C.; Heux, L.; Da Silva Perez, D.; Commandre, J.M.; Gourdon, C. Study of Solid Chemical Evolution in Torrefaction of Different Biomasses through Solid-State 13C Cross-Polarization/Magic Angle Spinning NMR (Nuclear Magnetic Resonance) and TGA (Thermogravimetric Analysis). *Energy* **2016**, *97*, 381–390. [CrossRef]
32. Saffe, A.; Fernandez, A.; Mazza, G.; Rodriguez, R. Prediction of Regional Agro-Industrial Wastes Characteristics by Thermogravimetric Analysis to Obtain Bioenergy Using Thermal Process. *Energy Explor. Exploit.* **2019**, *37*, 544–557. [CrossRef]
33. Zhou, H.; Long, Y.; Meng, A.; Li, Q.; Zhang, Y. The Pyrolysis Simulation of Five Biomass Species by Hemi-Cellulose, Cellulose and Lignin Based on Thermogravimetric Curves. *Thermochim. Acta* **2013**, *566*, 36–43. [CrossRef]
34. Wang, H.; Wang, X.; Cui, Y.; Xue, Z.; Ba, Y. Slow Pyrolysis Polygeneration of Bamboo (Phyllostachys Pubescens): Product Yield Prediction and Biochar Formation Mechanism. *Bioresour. Technol.* **2018**, *263*, 444–449. [CrossRef]
35. Naik, S.; Goud, V.V.; Rout, P.K.; Jacobson, K.; Dalai, A.K. Characterization of Canadian Biomass for Alternative Renewable Biofuel. *Renew Energy* **2010**, *35*, 1624–1631. [CrossRef]
36. Wang, S.; Zou, C.; Yang, H.; Lou, C.; Cheng, S.; Peng, C.; Wang, C.; Zou, H. Effects of Cellulose, Hemicellulose, and Lignin on the Combustion Behaviours of Biomass under Various Oxygen Concentrations. *Bioresour. Technol.* **2021**, *320*, 124375. [CrossRef]
37. Pasangulapati, V.; Ramachandriya, K.D.; Kumar, A.; Wilkins, M.R.; Jones, C.L.; Huhnke, R.L. Effects of Cellulose, Hemicellulose and Lignin on Thermochemical Conversion Characteristics of the Selected Biomass. *Bioresour. Technol.* **2012**, *114*, 663–669. [CrossRef]
38. Sengupta, D.; Pike, R.W. *Chemicals from Biomass: Integrating Bioprocesses into Chemical Production Complexes for Sustainable Development*; CRC Press: Boca Raton, FL, USA, 2012.
39. Krerkkaiwan, S.; Buranatrevedhya, S.; Sanduang, J.; Fukuda, S. Combustion Characteristics and Fouling Tendency of Co-Combustion between Sub-Bituminous Coal and Thai Biomass. In Proceedings of the Combustion Charazcteristics and Fouling Tendency of Co-Combustion between Sub-Bituminous Coal and Thai Biomass, 9th i-CIPEC, Kyoto, Japan, 21–23 September 2016.
40. Raj, T.; Kapoor, M.; Gaur, R.; Christopher, J.; Lamba, B.; Tuli, D.K.; Kumar, R. Physical and Chemical Characterization of Various Indian Agriculture Residues for Biofuels Production. *Energy Fuels* **2015**, *29*, 3111–3118. [CrossRef]

41. Dhyani, V.; Bhaskar, T. A Comprehensive Review on the Pyrolysis of Lignocellulosic Biomass. *Renew Energy* **2018**, *129*, 695–716. [CrossRef]
42. Mohammed, I.Y.; Abakr, Y.A.; Kazi, F.K.; Yusup, S.; Alshareef, I.; Chin, S.A. Comprehensive Characterization of Napier Grass as a Feedstock for Thermochemical Conversion. *Energies* **2015**, *8*, 3403–3417. [CrossRef]
43. Singh, Y.D.; Mahanta, P.; Bora, U. Comprehensive Characterization of Lignocellulosic Biomass through Proximate, Ultimate and Compositional Analysis for Bioenergy Production. *Renew Energy* **2017**, *103*, 490–500. [CrossRef]
44. Wannapeera, J.; Worasuwannarak, N.; Pipatmanomai, S. Product Yields and Characteristics of Rice Husk, Rice Straw and Corncob during Fast Pyrolysis in a Drop-Tube/Fixed-Bed Reactor. *Songklanakarin J. Sci. Technol.* **2007**, *30*, 393–404.
45. Nanda, S. *Conversion of Lignocellulosic Feedstocks to Renewable Fuels*; York University: Toronto, ON, Canada, 2013.
46. Hernandez-Mena, L.E.; Pecora, A.A.B.; Beraldo, A.L. Slow Pyrolysis of Bamboo Biomass: Analysis of Biochar Properties. *Chem. Eng. Trans.* **2014**, *37*, 115–120. [CrossRef]
47. Greenhalf, C.E.; Nowakowski, D.J.; Bridgwater, A.V.; Titiloye, J.; Yates, N.; Riche, A.; Shield, I. Thermochemical Characterisation of Straws and High Yielding Perennial Grasses. *Ind. Crops Prod.* **2012**, *36*, 449–459. [CrossRef]
48. Halder, P.; Kundu, S.; Patel, S.; Parthasarathy, R.; Pramanik, B.; Paz-Ferreiro, J.; Shah, K. TGA-FTIR Study on the Slow Pyrolysis of Lignin and Cellulose-Rich Fractions Derived from Imidazolium-Based Ionic Liquid Pre-Treatment of Sugarcane Straw. *Energy Convers. Manag.* **2019**, *200*, 112067. [CrossRef]
49. Guida, M.Y.; Lanaya, S.; Rbihi, Z.; Hannioui, A. Thermal Degradation Behaviors of Sawdust Wood Waste: Pyrolysis Kinetic and Mechanism. *J. Mater. Environ. Sci.* **2019**, *10*, 742–755.
50. Rahardjo, B.S. Effect of gasifiyng agent (air+steam) injection towards syngas quality from rice husk gasification. *Int. J. Eng.* **2013**, *4*, 8269.
51. Aydinli, B.; Caglar, A. The Catalytic Effects of Potassium Dichromate on the Pyrolysis of Polymeric Mixtures Part II: Hazelnut Shell and Ultra-High Molecular Weight Polyethylene and Their Blend Cases. *World Acad. Sci. Eng. Technol. Int. J. Mater. Metall. Eng.* **2010**, *4*, 462–466.
52. Villegas, J.M.; Avila, H. Quick-Scan Estimating Model of Higher Heating Value of Oil Palm Empty Fruit Bunches Based on Ash from Proximate Analysis Data. *Ing. Investig.* **2014**, *34*, 33–38. [CrossRef]
53. Camacho, Y.M.; Bensaid, S.; Ruggeri, B.; Restuccia, L.; Ferro, G.; Mancini, G.; Fino, D. Valorisation of By-Products/Waste of Agro-Food Industry by the Pyrolysis Process. *J. Adv. Catal. Sci. Technol.* **2016**, *3*, 1–11.
54. Guida, M.Y.; Hannioui, A. Properties of Bio-Oil and Bio-Char Produced by Sugar Cane Bagasse Pyrolysis in a Stainless Steel Tubular Reactor. *Prog. Agric. Eng. Sci.* **2017**, *13*, 13–33. [CrossRef]
55. Lyu, G.; Wu, S.; Zhang, H. Estimation and Comparison of Bio-Oil Components from Different Pyrolysis Conditions. *Front. Energy Res.* **2015**, *3*, 28. [CrossRef]
56. Ramos-Carmona, S.; Martínez, J.D.; Pérez, J.F. Torrefaction of Patula Pine under Air Conditions: A Chemical and Structural Characterization. *Ind. Crops Prod.* **2018**, *118*, 302–310. [CrossRef]
57. Park, S.; Kim, S.J.; Oh, K.C.; Cho, L.H.; Kim, D.H. Developing a Proximate Component Prediction Model of Biomass Based on Element Analysis. *Energies* **2023**, *16*, 509. [CrossRef]
58. Majumder, A.K.; Jain, R.; Banerjee, P.; Barnwal, J.P. Development of a New Proximate Analysis Based Correlation to Predict Calorific Value of Coal. *Fuel* **2008**, *87*, 3077–3081. [CrossRef]
59. Elmaz, F.; Yücel, Ö.; Mutlu, A.Y. Makine Öğrenmesi Ile Kısa ve Elemental Analiz Kullanarak Katı Yakıtların Üst Isı Değerinin Tahmin Edilmesi. *Int. J. Adv. Eng. Pure Sci.* **2020**, *32*, 145–151. [CrossRef]
60. Zhang, T.; Zhang, Q.; Wang, Q. Model Detection for Functional Polynomial Regression. *Comput. Stat. Data Anal.* **2014**, *70*, 183–197. [CrossRef]
61. Gendy, T.S.; El-Shiekh, T.M.; Zakhary, A.S. A Polynomial Regression Model for Stabilized Turbulent Confined Jet Diffusion Flames Using Bluff Body Burners. *Egypt. J. Pet.* **2015**, *24*, 445–453. [CrossRef]
62. Ivanovski, M.; Goricanec, D.; Krope, J.; Urbancl, D. Torrefaction Pretreatment of Lignocellulosic Biomass for Sustainable Solid Biofuel Production. *Energy* **2022**, *240*, 122483. [CrossRef]
63. Feng, Y.; Qiu, K.; Zhang, Z.; Li, C.; Rahman, M.M.; Cai, J. Distributed Activation Energy Model for Lignocellulosic Biomass Torrefaction Kinetics with Combined Heating Program. *Energy* **2022**, *239*, 122228. [CrossRef]
64. Zhang, Z.; Duan, H.; Zhang, Y.; Guo, X.; Yu, X.; Zhang, X.; Rahman, M.M.; Cai, J. Investigation of Kinetic Compensation Effect in Lignocellulosic Biomass Torrefaction: Kinetic and Thermodynamic Analyses. *Energy* **2020**, *207*, 118290. [CrossRef]
65. Garba, M.U.; Gambo, S.U.; Musa, U.; Tauheed, K.; Alhassan, M.; Adeniyi, O.D. Impact of Torrefaction on Fuel Property of Tropical Biomass Feedstocks. *Biofuels* **2018**, *9*, 369–377. [CrossRef]
66. Phanphanich, M.; Mani, S. Impact of Torrefaction on the Grindability and Fuel Characteristics of Forest Biomass. *Bioresour. Technol.* **2011**, *102*, 1246–1253. [CrossRef]
67. Meng, J.; Park, J.; Tilotta, D.; Park, S. The Effect of Torrefaction on the Chemistry of Fast-Pyrolysis Bio-Oil. *Bioresour. Technol.* **2012**, *111*, 439–446. [CrossRef]
68. Chan, Y.H.; Yusup, S.; Quitain, A.T.; Uemura, Y.; Sasaki, M. Bio-Oil Production from Oil Palm Biomass via Subcritical and Supercritical Hydrothermal Liquefaction. *J. Supercrit. Fluids* **2014**, *95*, 407–412. [CrossRef]

69. Manatura, K. Inert Torrefaction of Sugarcane Bagasse to Improve Its Fuel Properties. *Case Stud. Therm. Eng.* **2020**, *19*, 100623. [CrossRef]
70. Yang, W.; Shimanouchi, T.; Iwamura, M.; Takahashi, Y.; Mano, R.; Takashima, K.; Tanifuji, T.; Kimura, Y. Elevating the Fuel Properties of Humulus Lupulus, Plumeria Alba and *Calophyllum inophyllum* L. through Wet Torrefaction. *Fuel* **2015**, *146*, 88–94. [CrossRef]

Disclaimer/Publisher's Note: The statements, opinions and data contained in all publications are solely those of the individual author(s) and contributor(s) and not of MDPI and/or the editor(s). MDPI and/or the editor(s) disclaim responsibility for any injury to people or property resulting from any ideas, methods, instructions or products referred to in the content.